

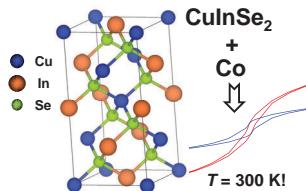
## Ferromagnetism in fast temperature quenched cobalt-doped chalcopyrites $\text{Cu}_{1-x/2}\text{In}_{1-x/2}\text{Co}_x\text{Se}_2$

Mikhail A. Zykin,\* Svetlana V. Golodukhina and Nikolay N. Efimov

*N. S. Kurnakov Institute of General and Inorganic Chemistry, Russian Academy of Sciences, 119991 Moscow, Russian Federation. Fax: +7 495 954 1279; e-mail: mzykin@gmail.com*

DOI: 10.1016/j.mencom.2023.02.038

**Synthetic conditions for cobalt-doped chalcopyrites  $\text{Cu}_{1-x/2}\text{In}_{1-x/2}\text{Co}_x\text{Se}_2$  were modified by adding a stage of fast temperature quenching from 1000 °C to cause significant ferromagnetism. Ferromagnetism persisted even at room temperature, and it was characterized by coercivity up to 140 Oe.**



**Keywords:** chalcopyrite, ferromagnetism, diluted magnetic semiconductors,  $\text{CuInSe}_2$ , cobalt.

Semiconductors with a chalcopyrite ( $\text{CuFeS}_2$ ) structure are compounds in the diamond-like tetrahedral structure of which each ion is surrounded by four counterions. This structure is a derivative of cubic  $\text{ZnS}$  with doubled unit cells. Among them are  $\text{CuGaSe}_2$ ,  $\text{CuInSe}_2$ , whose solid solutions known as CIGS are used as photovoltaic materials.<sup>1,2</sup> Thin-film solar cells based on them demonstrated a very high efficiency to 23%. At the same time, compounds with a chalcopyrite structure (II–IV–V<sub>2</sub> family like  $\text{CdGeP}_2$ <sup>3,4</sup>) doped with transition metal cations (primarily, manganese) have been actively studied as so-called diluted magnetic semiconductors. The diluted magnetic semiconductors<sup>5</sup> (primarily,  $\text{GaAs} : \text{Mn}^6$ ), being simultaneously semiconductors and ferromagnetics, are very promising for spintronic applications.<sup>7–9</sup> Both semiconducting and ferromagnetic properties of photovoltaic  $\text{CuMSe}_2$  ( $\text{M} = \text{Ga, In}$ ) materials are attractive. Ferromagnetism was theoretically predicted for transition metal-doped  $\text{CuMSe}_2$  chalcopyrites.<sup>10,11</sup> The compounds  $\text{CuGaSe}_2 : \text{Mn}^{12}$ ,  $\text{CuInSe}_2 : \text{Mn}^{13}$ , and  $\text{CuInSe}_2 : \text{Co}^{14}$  with doping levels to 10 at% were synthesized and magnetically characterized, but they were found paramagnetic. At the same time, a weak ferromagnetic signal was detected in  $\text{CuGaSe}_2 : \text{Mn}$  after rapid cooling of the sample due to an increase in the solubility of manganese.<sup>15</sup> Here, we report the occurrence of ferromagnetism in cobalt-doped  $\text{CuInSe}_2$  synthesized with quenching.

Cobalt-doped chalcopyrites  $\text{Cu}_{1-x/2}\text{In}_{1-x/2}\text{Co}_x\text{Se}_2$  with  $x = 0.06$  (sample 2), 0.08 (sample 3), 0.1 (sample 4), and 0.2 (sample 5) and, for comparison, pure  $\text{CuInSe}_2$  (sample 1) were synthesized by a two-step procedure of solid-state synthesis performed in evacuated quartz ampoules. At the first step, target compounds were synthesized from elemental Cu, In, Se, and Co with the subsequent slow cooling to room temperature; the obtained samples were mainly paramagnetic and demonstrated only traces of ferromagnetism.<sup>14</sup> The second step was similar to the first one, but it started from chalcopyrite compounds synthesized at the first step with the slow cooling and finished by the rapid quenching of ampoules from 1000 °C in water. Details of synthetic procedures can be found in Online Supplementary Materials.

According to X-ray diffraction (XRD) analysis, the samples were single-phase  $\text{CuInSe}_2$ . No impurity phases and noise signals of amorphous phases were found (Figures S2, S3). Electron-microscopic images of 4 also showed a homogeneous picture with no sign of impurities (Figures S8–S10). Chemical analysis performed by energy-dispersive X-ray (EDX) spectroscopy confirmed the stoichiometry of the nominal composition (Table S5). The unit cell parameters  $a$  and  $c$  and volume  $V$  [Figure 1(a), Table S1, Figure S4] decreased with the nominal cobalt content, as expected due to ionic radii relation ( $\text{Co}^{2+}$  with a radius of 0.56 Å is smaller than either  $\text{Cu}^+$  or  $\text{Ga}^{3+}$ , 0.60 or 0.47 Å, respectively<sup>16</sup>). At the same time, the cell parameters changed only slightly comparing with those of parent unquenched samples; that is, cobalt was incorporated in the chalcopyrite lattice in quantities

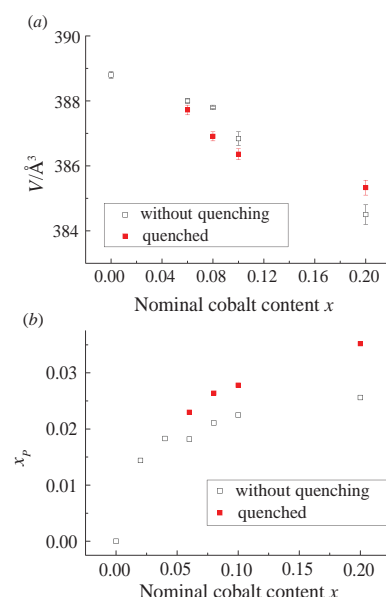


**Figure 1** (a) Unit cell volume  $V$  and (b) paramagnetic cobalt content  $x_p$  as functions of nominal cobalt content  $x$  in the synthesized (quenched) samples in comparison with those of parent unquenched<sup>14</sup> samples.

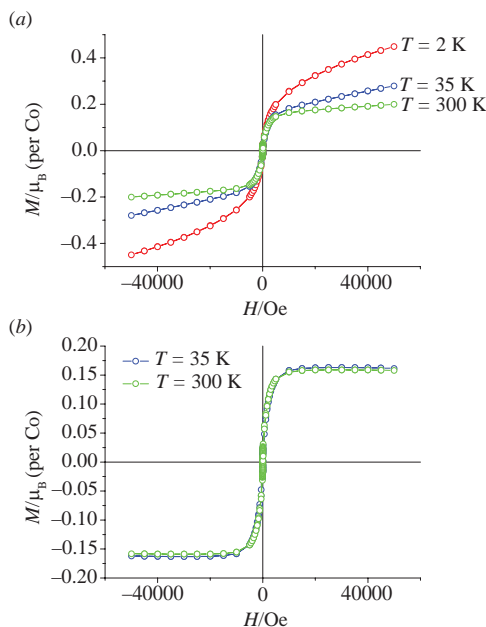


**Figure 2** (a) Isothermal magnetization curves measured at temperatures  $T = 2, 35, \text{ and } 300 \text{ K}$  and (b) ‘ferromagnetic’ isothermal magnetization curves for  $T = 35$  and  $300 \text{ K}$  obtained by the subtraction of linear parts from measured curves (see the text) for 5.

close to those in unquenched samples, whereas magnetic properties changed drastically.

The isothermal magnetization–magnetic field  $M(H)$  curves show a hysteretic behavior with a linear part [Figures 2(a), S5]. The subtraction of linear parts gave nearly identical hysteresis loops at  $T = 35$  and  $300 \text{ K}$  [Figures 2(b), S5] with saturation magnetization  $M_S$  of about  $900 \text{ emu mol}^{-1}$  per cobalt for 5 and coercive fields of 140 and 83 Oe at 35 and  $300 \text{ K}$ , respectively (see Online Supplementary Materials, Table S2).

Thus, all the samples demonstrated ferromagnetic behavior and  $M_S$  increased with the cobalt content; they were characterized by a coercive field of about 100–200 Oe even at room temperature (Figures 3, S6).

At the same time, the magnetic behavior of the samples was more complicated. The  $M(H)$  curves were a combination of a temperature-independent ferromagnetic signal and constant field-independent paramagnetic-like magnetic susceptibility  $\chi_{FIP}$ , which manifested itself as a linear part of  $M(H)$  (at  $T = 35$  and  $300 \text{ K}$ ; at  $2 \text{ K}$ , this linear part was curved apparently according to the Brillouin function). Note that this value of  $\chi_{FIP}$  does not obey the Curie–Weiss law (values at 35 and  $300 \text{ K}$  are much closer to each other than they should be).

The  $\chi T(T)$  curves for all the samples (Figure S7) demonstrated a strong linear dependence that means the presence of a temperature-independent contribution to the magnetic susceptibility  $\chi_{TIP}$ , most (but not all) of which is related to ferromagnetic constant magnetization. The remaining part of  $\chi_{TIP}$  is temperature and magnetic field-independent susceptibility  $\chi_{const}$ . After subtracting constant  $\chi_{TIP}$  from  $\chi T(T)$ , the remaining magnetic susceptibility  $\chi_{para}$  obeyed the Curie–

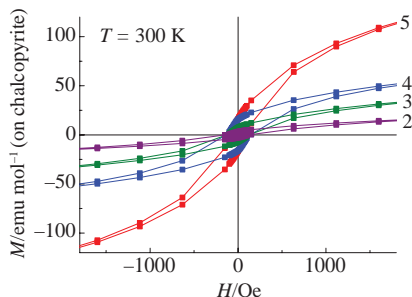


**Figure 3**  $M(H)$  hysteresis loops at  $T = 300 \text{ K}$  for  $\text{Cu}_{1-x/2}\text{In}_{1-x/2}\text{Co}_x\text{Se}_2$ ;  $x = 0.06$  (2), 0.08 (3), 0.1 (4), and 0.2 (5).

Weiss law (Figure S7, Table S3). Therefore, the magnetic properties include (1) an almost temperature-independent ferromagnetic part that increases with the cobalt content [hysteresis on  $M(H)$  dependences with pretty fast saturation; the main contribution to the temperature-independent part of the magnetic susceptibility  $\chi_{TIP}$ , observed on the  $\chi T(T)$  dependence]; (2) constant magnetic susceptibility  $\chi_{const}$  that does not depend on both temperature and magnetic field [part of  $\chi_{FIP}$  and  $\chi_{TIP}$ , is very close in all the samples if calculated per mole of cobalt and amounts to about  $0.0038 \text{ cm}^3 \text{ mol}^{-1}$  (Table S3), and could be for example related to magnetism of free charge carriers]; and (3) a conventional paramagnetic part  $\chi_{para}$  that obeys the Curie–Weiss law [part of  $\chi_{FIP}$ , temperature-dependent part of  $\chi(T)$ ]. Most likely, this  $\chi_{para}$  is caused by cobalt atoms incorporated in a chalcopyrite lattice. This paramagnetic cobalt content  $x_P$  was calculated from the Curie–Weiss law [Figure 1(b), Table S4]. As can be seen, this  $x_P$  content is similar for quenched and unquenched samples (slightly higher in the quenched samples) and also correlates with similar unit cell volumes [Figure 1(a)].

Thus, quenching caused the emergence of ferromagnetism in cobalt-doped  $\text{CuInSe}_2$  although the quantity of cobalt atoms incorporated in a chalcopyrite cell increased only slightly. It cannot be completely ruled out that this ferromagnetism was caused by a cobalt-containing impurity (but at least not  $\text{CoSe}_2$  or  $\text{Co}_3\text{Se}_4$  found in the unquenched samples without any ferromagnetic signal). Ferromagnetism persisted even at room temperature with a coercivity of 140 Oe.

This work was supported by the Russian Foundation for Basic Research, project no. 19-33-60080. This research was performed using the equipment of the JRC PMR IGIC RAS (a Bruker D8 Advance diffractometer, a PPMS-9 Quantum Design magnetometer, and a Carl Zeiss NVision 40 high-resolution scanning electron microscope).

#### Online Supplementary Materials

Supplementary data associated with this article can be found in the online version at doi:10.1016/j.mencom.2023.02.038.

#### References

1. A. Polman, M. Knight, E. C. Garnett, B. Ehrler and W. C. Sinke, *Science*, 2016, **352**, aad4424.
2. G. Regmi, A. Ashok, P. Chawla, P. Semalti, S. Velumani, S. N. Sharma and H. Castaneda, *J. Mater. Sci. Mater. Electron.*, 2020, **31**, 7286.
3. K. Sato, G. A. Medvedkin and T. Ishibashi, *J. Cryst. Growth*, 2002, **237–239**, 1363.
4. L. I. Koroleva, D. M. Zashchirinskii, T. M. Khapaeva, A. I. Morozov, S. F. Marenkin, I. V. Fedorchenko and R. Szymczak, *J. Magn. Magn. Mater.*, 2011, **323**, 2923.
5. T. Dietl, A. Bonanni and H. Ohno, *J. Semicond.*, 2019, **40**, 080301.
6. H. Ohno, *Science*, 1998, **281**, 951.
7. H. Ohno, D. Chiba, F. Matsukura, T. Omiya, E. Abe, T. Dietl, Y. Ohno and K. Ohtani, *Nature*, 2000, **408**, 944.
8. D. Chiba, H. Yamanouchi, F. Matsukura and H. Ohno, *Science*, 2003, **301**, 943.
9. H. Ohno, *Phys. B: Condens. Matter*, 2006, **376–377**, 19.
10. A. J. Freeman and Y.-J. Zhao, *J. Phys. Chem. Solids*, 2003, **64**, 1453.
11. Y.-J. Zhao and A. Zunger, *Phys. Rev. B: Condens. Matter Mater. Phys.*, 2004, **69**, 104422.
12. M. A. Zykin, E. V. Busheva, T. G. Aminov, G. G. Shabunina and N. N. Efimov, *Russ. J. Inorg. Chem.*, 2022, **67**, 150 (*Zh. Neorg. Khim.*, 2022, **67**, 168).
13. J. Yao, C. N. Kline, H. Gu, M. Yan and J. A. Aitken, *J. Solid State Chem.*, 2009, **182**, 2579.
14. M. A. Zykin and N. N. Efimov, *Russ. Chem. Bull.*, 2022, **71**, 701.
15. M. A. Zykin and N. N. Efimov, *Inorg. Mater.*, 2022, **58**, 18 (*Neorg. Mater.*, 2022, **58**, 21).
16. CRC Handbook of Chemistry and Physics, 84<sup>th</sup> edn., ed. D. R. Lide, CRC Press, Boca Raton, 2003.

Received: 31st October 2022; Com. 22/7035